ACS APPLIED MATERIALS & INTERFACES

Research Article

www.acsami.org

Synthesis of Raspberry-Like SiO_2–TiO_2 Nanoparticles toward Antireflective and Self-Cleaning Coatings

Xiaoyu Li[†,‡,§] and Junhui He*[,†]

[†]Functional Nanomaterials Laboratory and Key Laboratory of Photochemical Conversion and Optoelectronic Materials, Technical Institute of Physics and Chemistry, Chinese Academy of Sciences (CAS), 29 Zhongguancundonglu, Haidianqu, Beijing 100190, China

[‡]University of Chinese Academy of Sciences, Beijing 100864, China

[§]Key Laboratory of Green Process and Engineering, Institute of Process Engineering, Chinese Academy of Sciences, Beijing 100190, China

Supporting Information

ABSTRACT: Silica–titania core–shell nanoparticles of 30, 40, 50, 55, 75, and 110 nm were prepared from tetraethyl orthosilicate (TEOS) and tetraisopropyl titanate (TIPT). After calcination, the amorphous titania shell transformed into anatase nanoparticles, and the silica–titania core–shell nanoparticles became raspberry-like nanoparticles. These nanoparticles were characterized by scanning electron microscopy (SEM), transmission electron microscopy (TEM), thermogravimetric analysis (TGA), X-ray diffraction (XRD), Fourier transform infrared (FT-IR) spectroscopy, and UV–vis spectroscopy. Hierarchically structured antireflective and self-cleaning particulate coatings were fabricated on glass substrates via layer-by-layer (LbL) assembly using silica–titania core–shell nanoparticles and silica nanoparticles as building blocks followed by calcination. The maximum transmittance of coated glass substrates reached as high as ca. 97%, while that of the glass substrates is only ca. 91%. The morphologies of the coatings were observed by SEM and atom force microscopy (AFM). Such hierarchically structured raspberry-like SiO_2–TiO_2 nanoparticle coatings had superhydrophilic and antifogging properties. The coatings also showed photocatalytic activity toward organic pollutants and thus a self-cleaning property.

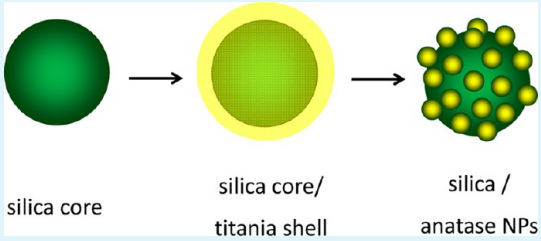

KEYWORDS: *raspberry-like silica-tiania nanoparticle, LbL self-assembly, superhydrophilic, antifogging, photodegradation, self-cleaning*

1. INTRODUCTION

Titanium dioxide (TiO_2) has attracted great attention of scientists for years because of its interesting physical and chemical properties. It has been applied to many fields, such as dye-sensitized solar cells,[1−6] water splitting into H_2 devices,[7−11] photocatalytic degradation of organic polutants,[12−17] and antibacterial coatings.[18,19] Among a variety of applications, the utilization of TiO_2 in self-cleaning coatings, which make use of sunlight and natural rainfall to keep surfaces clean, is one of the most attractive and promising fields.[20,21] The self-cleaning coatings have been commercially attractive and available in the building industry currently, since it can save significant cost for maintenance. The mechanism of self-cleaning is that anatase TiO_2 coatings with high photoactivity can decompose organic contaminants and induce its surface hydrophilicity under UV illumination.[22−24] Unfortunately, TiO_2 has a high refractive index ($n \approx 2.52$ for anatase), and thus, when it is applied as antireflective and self-cleaning coatings to solar cells, green houses, and windows of tall buildings, the percentage of TiO_2 must be kept low enough to lower the refractive index of whole coatings.[25] However, the low TiO_2 content is unfavorable for the self-cleaning property. Therefore, the fabrication of self-cleaning antireflective TiO_2 coatings has been widely studied toward balancing the photocatalytic and transmission properties. A general method is to prepare the composite of TiO_2 and another material with a low refractive index such as SiO_2 ($n \approx 1.5$).[26]

Layer-by-layer (LbL) assembly has already proved to be a simple, convenient, and environment-benign method for design and fabrication of antireflective and self-cleaning coatings with tailored chemical composition and controllable architecture on varied substrate surfaces.[27−32] Self-cleaning and antireflective coatings were prepared by LbL assembly using TiO_2 nanoparticles and SiO_2 submicrometer particles as building blocks.[25] Fujishima and co-workers used SiO_2 nanoparticles and titanate nanosheets to fabricate self-cleaning coatings.[27] Rubner et al. fabricated antireflective and self-cleaning coatings via LbL deposition of charged TiO_2 and SiO_2 nanoparticles.[28] However, TiO_2 nanoparticles prepared by traditional routes, such as the sol–gel process and emulsion precipitation, usually have low crystallinity and need further calcination to have high photocatalytic activity.[33−35] Nevertheless, heat treatment can

Received: March 28, 2013
Accepted: May 17, 2013
Published: May 29, 2013

   dx.doi.org/10.1021/am401124j | ACS Appl. Mater. Interfaces 2013, 5, 5282−5290

Table 1. Preparation of SiO_2−TiO_2 Nanoparticles of Varied Sizes without Calcination

	TEOS (mL)	EtOH (mL)	NH_3 H_2O 25% (mL)	H_2O (mL)	T (°C)	TIPT (mL)	d_n[a] (nm)	d_c[b] (nm)	S[c] (nm)
ST30	2.3	60	3	0	50	2.9	30.3	28.6	2.7
ST40	2.3	60	3	0	40	2.9	42.3	31.3	3.1
ST50	2.3	60	3	1	50	2.9	49.8	42.2	7.5
ST55	2.3	60	3	0	30	2.9	56.0	51.6	4.6
ST75	2.3	60	3	1	40	2.9	76.8	72.5	6.4
ST110	2.3	60	3	1	30	2.9	111.4	105.4	9.8

[a] d_n is the average size of SiO_2−TiO_2 nanoparticles without calcination by measuring at least 50 individual nanoparticles for each sample on the corresponding TEM images. [b] d_c is the average size of the SiO_2 core of SiO_2−TiO_2 nanoparticles by measuring at least 50 individual nanoparticles for each sample on the corresponding TEM images. With a decrease of reaction temperature, the particle size increases, which may be due to slower hydrolysis at lower temperature, and when 1 mL of water was added under otherwise identical conditions, the particle size increases, which may be due to quick growth of particles. [c] S is the standard deviation of variance of particle size (d_n) distribution: $S = (\Sigma(d_i - d_n)^2/\Sigma n_i)^{1/2}$.

cause particle agglomeration and particle size change. Such changes are harmful to the photocatalytic property of coatings. Thus, preparation of coatings with well-dispersed TiO_2 nanoparticles and thus high antireflective and photocatalytic self-cleaning properties is still a big challenge.

Here, we prepared a series of raspberry-like SiO_2−TiO_2 nanoparticles by the one-pot sol−gel method. The size of TiO_2 nanoparticles on the surface of the SiO_2 core can be tailored by regulating the molar ratio of tetraethyl orthosilicate (TEOS)/tetraisopropyl titanate (TIPT), and by immobilization on the SiO_2 core, these tiny TiO_2 nanoparticles could keep high specific surface area without aggregation. The small TiO_2 particles, in the structure of raspberry-like SiO_2−TiO_2 nanoparticles, were of the anatase phase, which shows high photocatalytic activity. Highly antireflective and photocatalytic self-cleaning coatings were prepared via LbL assembly with SiO_2−TiO_2 core−shell nanoparticles followed by calcination, which transformed the TiO_2 shell into anatase nanoparticles without agglomeration. The maximum transmittance of coating reached as high as 97.3%. These coatings exhibited superhydrophilic property both with and without UV illumination. The self-cleaning property of coating was observed by photocatalytic degradation of methylene blue adsorbed on the coating. To our best knowledge, there have been few reports about antireflective and self-cleaning coatings prepared from in situ formed raspberry-like SiO_2−TiO_2 nanoparticles via layer-by-layer assembly.

2. EXPERIMENTAL SECTION

2.1. Materials. Tetraethyl orthosilicate (TEOS, 99+%), sodium poly(4-styrenesulfonate) (PSS, M_w = 70 000), and tetraisopropyl titanate (TIPT, 97%) were obtained from Alfa Aesar. Poly(diallyldimethylammonium chloride) (PDDA, M_w = 200 000−350 000, 20 wt %) was purchased from Aldrich. Methylene blue (MB, > 98%), aqueous ammonia (25%), concentrated sulfuric acid (98%), hydrogen peroxide (30%), and absolute ethanol (99.5%) were purchased from Beihua Fine Chemicals. Ultrapure water with a resistivity higher than 18.2 MΩ·cm was used in all experiments and was obtained from a three-stage Millipore Mill-Q Plus 185 purification system (Academic).

2.2. Synthesis of Monodisperse SiO_2 Nanospheres and SiO_2−TiO_2 Core−Shell Nanoparticles. Monodisperse SiO_2 nanoparticles of ca. 20 nm (S-20) and monodisperse SiO_2 nanoparticles of other varied sizes as the cores of SiO_2−TiO_2 nanoparticles (Table 1) were prepared according to the Stöber method.[36] The pH values of the SiO_2 suspensions were ca. 10.

For a typical synthesis of SiO_2−TiO_2 nanoparticles, 2.3 mL of TEOS was added to a mixed solution of aqueous ammonia (3.0 mL), ultrapure water (1.0 mL), and ethanol (60 mL) at 40 °C. The mixture was stirred at 40 °C for an additional 6 h. It was further stirred at room temperature for 2 h, and the pH value of the solution decreased to 7. Then, 2.9 mL of TIPT was added to the above solution to coat the obtained silica nanoparticles with a titania layer. The solution was stirred at room temperature for an additional 6 h. Synthesis conditions of SiO_2−TiO_2 nanoparticles of varied sizes and the diameters of resulting nanoparticles are shown in Table 1. The SiO_2−TiO_2 core−shell nanoparticles with a diameter of 30.3, 42.3, 49.8, 56.0, 76.8, and 111.4 nm, which were measured before calcination, are denoted as ST30, ST40, ST50, ST55, ST75, and ST110, respectively. The prepared SiO_2−TiO_2 core−shell nanoparticles were collected by centrifugation (10 000 rpm, 5 min) and redispersed in absolute ethanol for suspensions of 0.1 wt % SiO_2−TiO_2 core−shell nanoparticles, and their pH values were adjusted to 1−2 by adding a certain volume of hydrochloric acid (26−28%).

2.3. Thin Film Assembly. The fabrication process of superhydrophilic and antireflective coatings is described as follows. First, glass substrates were cleaned with Piranha solution (98 wt % H_2SO_4/30 wt % H_2O_2, 7/3 v/v) and then washed with water. (*Caution*: the Pirhana solution is highly dangerous and must be used with great care.) The cleaned substrates were alternately dipped in PDDA and PSS solutions for 5 min, and redundant polyelectrolytes were removed by shaking in pure water for 2 min and rinsing for 1 min followed by drying with N_2 flow. The concentrations of PDDA and PSS aqueous solutions were 2 mg mL^{-1}. Multilayers of $(PDDA/PSS)_5$/PDDA were prepared and were used as a primer in all experiments. Second, the $(PDDA/PSS)_5$/PDDA covered substrates were alternately dipped in a prepared 20 nm SiO_2 suspension (0.1 wt %) and an PDDA solution (2 mg mL^{-1}) or SiO_2−TiO_2 core−shell nanoparticle suspension (0.1 wt %) by the same procedure for an appropriate number of cycles. Finally, the as-prepared coatings were blown dry with pure N_2 flow at room temperature and calcinated (heating rate: 10 °C min^{-1}) at 550 °C for 3 h.

2.4. Characterization. For transmission electron microscopy (TEM) observations, powder samples were added on carbon-coated copper grids and observed on a JEOL JEM-2100F transmission electron microscope at an acceleration voltage of 200 kV. Freshly fabricated coatings were examined by scanning electron microscopy (SEM) on a Hitachi S-4300 scanning electron microscope operated at 10 kV. Fourier transform infrared (FT-IR) spectra were collected on a Varian Excalibur 3100 FT-IR spectrometer. X-ray diffraction (XRD) patterns of the obtained ST75 nanoparticles before and after calcination at 400 or 550 °C for 3 h were recorded on a Bruker D8 Focus X-ray diffractometer using Cu Kα radiation (λ = 0.1542 nm) operated at 40 kV and 40 mA. Thermogravimetric analysis (TGA) and differential scanning calorimetry (DSC) analysis of the prepared ST75 nanoparticles before calcination were performed on a SDTQ-600 thermalgravimetric analyzer (TA Instruments) at a heating rate of 10 °C/min from 20 to 700 °C under an air flow. Transmission and absorption spectra in the wavelength range of 300−800 nm were recorded using a TU-1901 spectrophotometer (Beijing Purkinje General Instrument Co.). Reflection spectra were identified on a Varian Cary 5000 UV/vis-NIR spectrophotometer. Water contact angles (WCAs) of coating surfaces were measured at ambient temperature on a JC2000C contact angle/interface system (Shanghai

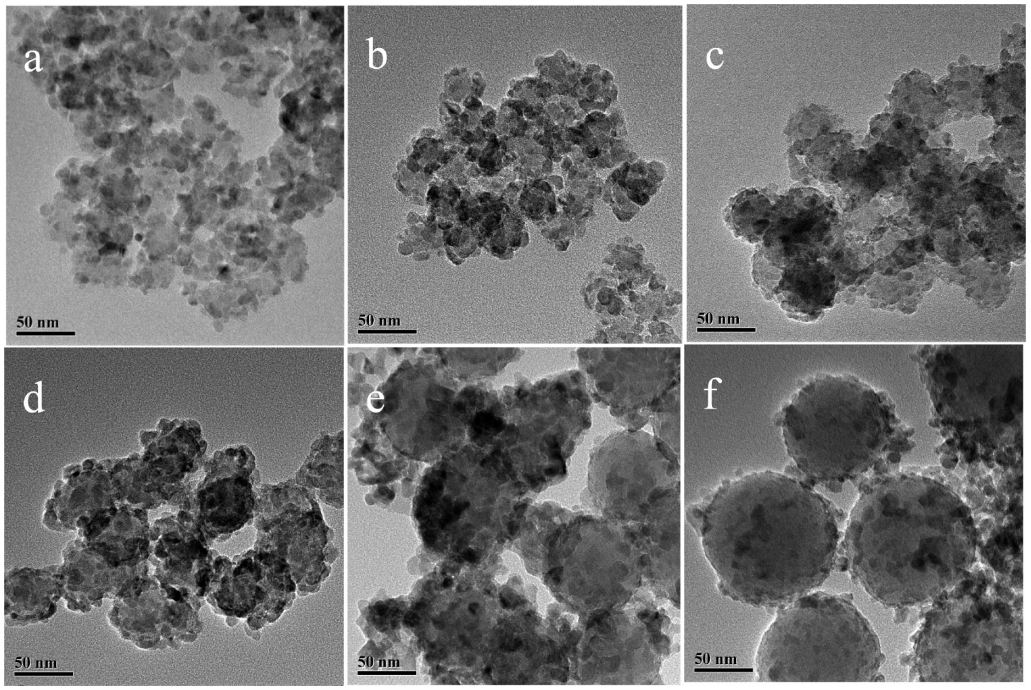

Figure 1. TEM images of SiO_2−TiO_2 raspberry-like nanoparticles of ST30 (a), ST40 (b), ST50 (c), ST55 (d), ST75 (e), and ST110 (f) with a silica core of 28.6, 31.3, 42.2, 47.8, 72.5, and 105.4 nm, respectively, after calcination at 550 °C for 3 h.

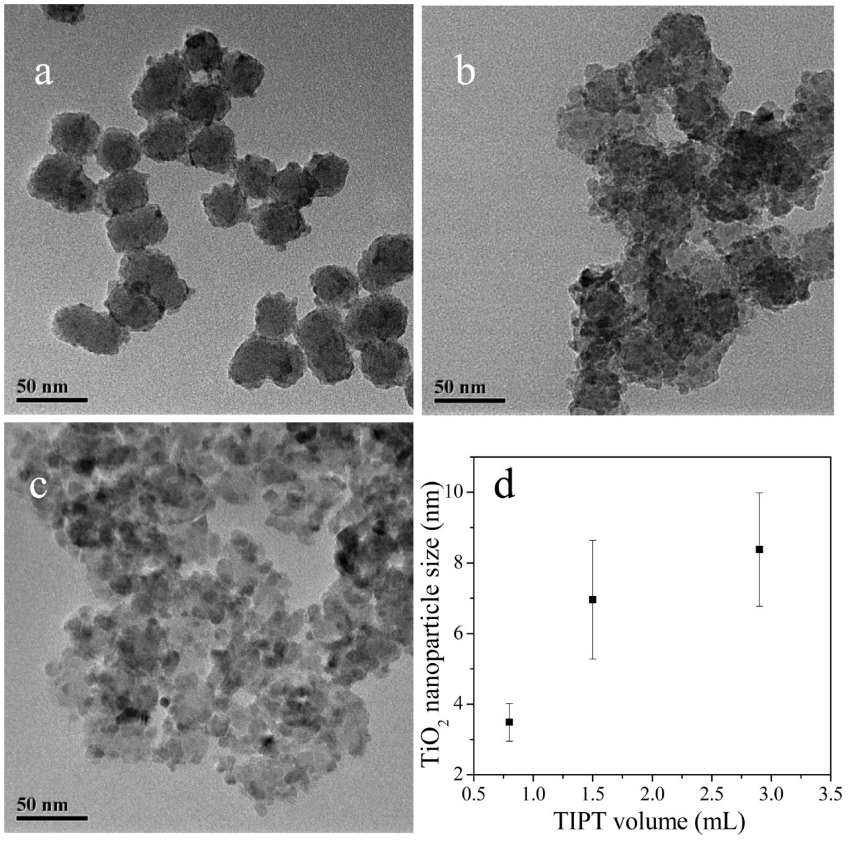

Figure 2. TEM images of SiO_2−TiO_2 raspberry-like nanoparticles with a 28.6 nm SiO_2 core obtained by adding a TIPT volume of 0.8 mL (a), 1.5 mL (b), and 2.9 mL (c), respectively, followed by calcination at 550 °C for 3 h. (d) Correlation between TiO_2 particle size and TIPT volume.

Zhongchen Digital Technique Apparatus Co.). Water droplets of 4 μL were dropped carefully onto sample surfaces. For examination of antifogging property, a control slide glass and a slide glass with antireflevtive coating were cooled at ca. −15 °C for 3 h in a refrigerator and then exposed to humid laboratory air (relative humidity ca. 50% RH).

2.5. Adsorption and Photocatalytic Degradation. The self-cleaning property was evaluated by investigating the adsorption and

dx.doi.org/10.1021/am401124j | ACS Appl. Mater. Interfaces 2013, 5, 5282−5290

photocatalytic degradation of methylene blue. A methylene blue stock solution of 10 mg/L was prepared. UV-irradiation was provided by a high pressure mercury lamp (250 W) through a thick transparent jacket with circulating-water to cool the lamp and remove the effect of heat. The ST75 raspberry-like nanoparticles obtained after calcination at 550 °C were added in a MB solution of 10 mg/L in a quartz container under stirring for 2 h in the dark to reach saturated adsorption, and then, under the UV irradiation, the degradation of MB by the ST75 raspberry-like nanoparticles obtained after calcination at 550 °C was monitored by the absorption of MB solution after filtering the nanoparticles. Both slide glass with prepared thin coating and control slide glass were dipped in a MB solution of 10 mg/L for 5 min and then lifted at a constant withdrawal speed of 100 mm/min and dried in air. MB-adsorbed SiO_2–TiO_2 thin films were subjected to the UV irradiation. The decomposition of MB adsorbed by the SiO_2–TiO_2 thin film was monitored on the basis of the gradual disappearance of the MB peak in the transmission spectrum using a TU-1901 spectrophotometer.

3. RESULTS AND DISCUSSION

3.1. Effects of the TEOS/TIPT Molar Ratio on the Morphology and Structure of SiO_2–TiO_2 Nanoparticles. Raspberry-like SiO_2–TiO_2 nanoparticles were prepared by TEOS hydrolysis that was catalyzed by aqueous ammonia and then TIPT hydrolysis via the sol–gel process followed by calcination. Figure 1 shows TEM images of raspberry-like SiO_2–TiO_2 nanoparticles with varied sizes, which were prepared from different SiO_2 cores using varied TEOS contents but identical TIPT volume. The synthetic conditions are shown in Table 1. TEM images of these nanoparticles before and after calcination are available, respectively, in the Supporting Information (Figure S1–S6). It is noted that, with the same TIPT volume of 2.9 mL (TEOS/TIPT molar ratio 1:1), the size of SiO_2 (core)–TiO_2 (shell) nanoparticle is very dependent on the size of SiO_2 core, though the thickness of the TiO_2 shell becomes slightly thicker with a decrease of the SiO_2 core size. The diameters of SiO_2–TiO_2 core–shell nanoparticles of ST30, ST40, ST50, ST55, ST75, and ST110 before calcination were estimated to be 30.3, 42.3, 49.8, 56.0, 76.8, and 111.4 nm, respectively. In order to achieve good photocatalytic property, the core–shell nanoparticles were calcined at 550 °C for 3 h, producing crystalline TiO_2 shells. As revealed in Figure 1, after calcination, the TiO_2 shell became reconstructed with secondary TiO_2 nanoparticles of ca. 9 nm in size. Interestingly, when the TEOS/TIPT molar ratio was set at 1:1, TiO_2 nanoparticles did not significantly change in diameter but just changed in their coverage on the silica cores of varied sizes.

In order to regulate the TiO_2 nanoparticle size, we also prepared SiO_2–TiO_2 core–shell nanoparticles using identical TEOS volume (2.3 mL) but varied TIPT volumes. Varied TIPT volumes of 0.8 mL (TEOS/TIPT molar ratio 4:1), 1.5 mL (TEOS/TIPT molar ratio 2:1), and 2.9 mL (TEOS/TIPT molar ratio 1:1) were added, respectively, to 30 nm SiO_2 core nanoparticles. Figure 2a–c shows TEM images of obtained SiO_2–TiO_2 nanoparticles after calcination at 550 °C for 3 h. The average TiO_2 nanoparticle size was estimated from TEM images to be 3.5 ± 0.5, 7.0 ± 1.7, and 8.4 ± 1.6 nm, respectively, for the TEOS/TIPT molar ratios of 4:1, 2:1, and 1:1. Clearly, the average TiO_2 nanoparticle size and its standard deviation increase with a decrease of the TEOS/TIPT molar ratio (Figure 2d). Because the TiO_2 nanoparticles were highly dispersed on the SiO_2 nanoparticle, their agglomeration was hindered, and thus, the TiO_2 nanoparticles have a small average size and narrow size distribution. When the TEOS/TIPT molar ratio decreased to 4:1, the TiO_2 nanoparticle size decreased to 3.5 nm. At this TEOS/TIPT molar ratio, only a small number of crystallites formed on the surface of SiO_2 core, which were not sufficient to fully cover the SiO_2 nanoparticle surface until the molar TEOS/TIPT ratio reached 2:1.

As a building block for antireflective coatings, on one hand, it is better that the nanoparticle size is smaller than $\lambda/4$ of incident light.[27] On the other hand, in order to achieve good photocatalytic property, it is hoped that TiO_2 nanoparticles cover the SiO_2 nanoparticle surface as much as possible. Comparing all the obtained raspberry-like SiO_2–TiO_2 nanoparticles after calcination at 550 °C for 3 h, those of ST75 after calcination at 550 °C for 3 h (Figure 1e) have an ideal size and coverage of TiO_2 nanoparticles for the self-assembly of coatings. Thus, ST75 was analyzed and discussed below.

ST75 nanoparticles before and after calcination were characterized by FT-IR and UV–vis absorption spectra. The peak at 948 cm^{-1} in Figure S7 (Supporting Information) curve c corresponds to the vibration of Ti–O–Si, confirming the presence of Ti–O–Si in raspberry-like SiO_2–TiO_2 nanoparticles of ST75. The peak at 1403 nm was observed only in the spectrum for SiO_2–TiO_2 core–shell nanoparticles before calcination, which is due to the alkyl group of unreacted TIPT (C–H). The peak at 3000–3500 cm^{-1} was assigned to the Si–OH, Ti–OH, and H–OH. 1640 cm^{-1} peak was assigned to H_2O. Figure S7 (Supporting Information) curves b and c have more intense peaks both at 3500 and 1640 cm^{-1} because of the presence of H_2O. Figure S8 (Supporting Information) depicts the absorption spectra of original 75 nm SiO_2 nanoparticles, as-prepared SiO_2–TiO_2 nanoparticles, and SiO_2–TiO_2 nanoparticles after calcination. The SiO_2–TiO_2 nanoparticles before calcination show red-shifted absorption characteristics compared to the SiO_2 nanoparticles, agreeing with the formation of TiO_2 phase on the SiO_2 core. The results also agree with the TEM results.

3.2. Thermalgravimetric and XRD Analyses of SiO_2–TiO_2 Nanoparticles. Figure 3 represents TGA and DSC

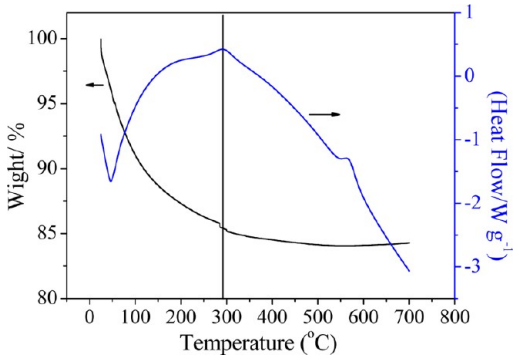

Figure 3. TGA-DSC curves of ST75 raspberry-like nanoparticles before calcination.

curves (heating rate: 10 °C/min, under air flow) of ST75 nanoparticles before calcination. The major weight loss occurred in the range of 40–100 °C on the TGA curve, which corresponds to an endothermic peak on the DSC curve and was due to evaporation of water. The second weight loss occurred at 290 °C while there was an exothermic peak on the DSC curve, indicating combustion of organic compounds. Beyond 290 °C, there was a slight weight loss, and at 563 °C,

dx.doi.org/10.1021/am401124j | ACS Appl. Mater. Interfaces 2013, 5, 5282–5290

there was an exothermic peak on the DSC curve, which might be attributed to the phase transition from amorphous TiO_2 to crystalline TiO_2. The deduction was supported by XRD patterns of ST75 nanoparticles (Figure S9 in the Supporting Information). The effect of calcination temperature was examined by XRD on the TiO_2 structure of ST75. Figure S9 (Supporting Information) indicates that TiO_2 of ST75 calcined at 400 °C was of the amorphous phase. After 550 °C calcination, however, it changed from the amorphous phase to the anatase phase. No rutile phase was observed.[37,38] It was reported that the transformation from anatase to rutile occurs in the higher temperature range of 700−800 °C.[39] On the basis of the TGA, DSC, and XRD analyses, we chose the "550 °C for 3 h" as the heat treatment conditions for preparing raspberry-like SiO_2−TiO_2 nanoparticles with TiO_2 of the anatase phase, which is well-known to have good photocatalytic activity.

XRD patterns could also be used to estimate the size of crystallites according to the Scherrer equation:

$$D = 0.89\lambda/(\beta\cos\theta) \quad (1)$$

where 2θ is the diffraction angle, λ is the wavelength of X-ray radiation, and β is the full width at the half-maximum of the diffraction peak.[40] The crystallite size of ST75 nanoparticles after calcination at 550 °C for 3 h was thus determined by measuring the (101) peak in the diffraction patterns, and it was calculated to be about 9.8 nm, nearly agreeing with the results by TEM observations.

3.3. Photocatalytic Property of Raspberry-Like SiO_2−TiO_2 Nanoparticles. There are many Ti−OH groups on the surface of raspberry-like SiO_2−TiO_2 nanoparticles, and the point of zero charge (PZC) is 5.5 for TiO_2.[25] At a pH value lower than the PZC of titania (pH < PZC), the particle surface becomes positively charged (eq 2), whereas at pH > PZC, it becomes negatively charged (eq 3).

$$TiOH + H^+ = TiOH_2^+ \quad (2)$$

$$TiOH + OH^- = TiO^- \quad (3)$$

Since MB has a cationic configuration, its adsorption on raspberry-like SiO_2−TiO_2 nanoparticles is favorable in neutral solution.[41] Thus, raspberry-like SiO_2−TiO_2 nanoparticles of ST75 after calcination at 550 °C for 3 h were added in the MB solution under stirring, and the mixture was stirred for an additional 2 h in the dark to reach saturation adsorption. In absence of raspberry-like SiO_2−TiO_2 nanoparticles of ST75 after calcination at 550 °C for 3 h, no degradation occurred under UV-irradiation (Figure S10 in the Supporting Information). However, photocatalytic degradation of MB was observed under identical UV irradiation in the presence of raspberry-like SiO_2−TiO_2 nanoparticles of ST75 after calcination at 550 °C for 3 h. As shown in Figure 4a, the raspberry-like SiO_2−TiO_2 nanoparticles of ST75 after calcination at 550 °C for 3 h could effectively degrade MB. The change in absorbance at 670 nm was chosen to characterize the decoloration of MB, and the photocatalytic degradation of MB is shown as a function of irradiation time in Figure 4b. Thus, under UV irradiation, the percentage of degradation reached 87.1% after 20 min in the presence of raspberry-like SiO_2−TiO_2 nanoparticles of ST75 nanoparticles after calcination at 550 °C for 3 h, whereas it was almost 0% under identical UV irradiation for the same period of time in the absence of the nanoparticles (Figure S10 in the Supporting Information). The reaction kinetics was found to follow an apparent first-order kinetics

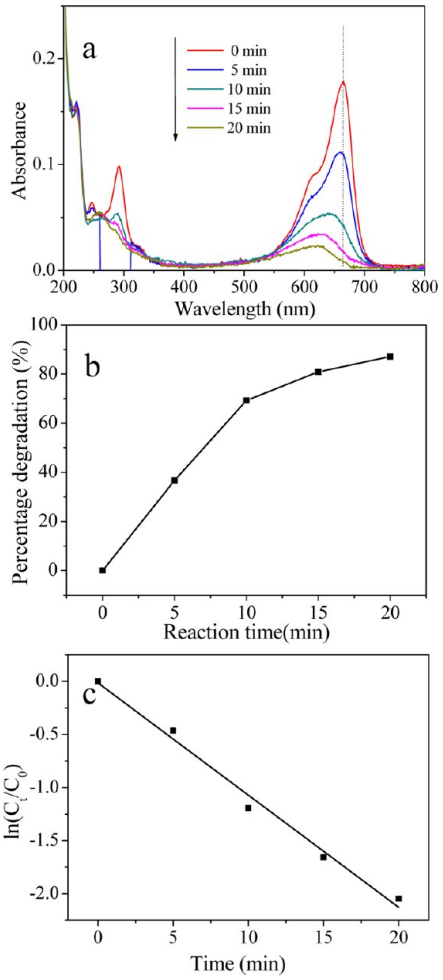

Figure 4. (a) Time-dependent UV−vis absorption spectral changes of the reaction mixture containing 10 mL of aqueous MB of 10 mg/L and photocatalyzed by ST75 raspberry-like nanoparticles. (b) Degradation efficiency of ST75 raspberry-like nanoparticles. (b) Plot of $\ln(C_t/C_0)$ versus reaction time.

($\ln(C_0/C_t) = K_{app}t$) (Figure 4c), and the K_{app} value was estimated to be $1.76 \times 10^{-3}s^{-1}$ ($R^2 = 0.985$). The above results indicate that raspberry-like SiO_2−TiO_2 nanoparticles of ST75 after calcination at 550 °C for 3 h have good photocatalytic activity. The reason may be that the small titania nanoparticles loaded on the silica core possess high surface area and imperfect anatase phase, which produces abundant electron−hole pairs under UV irradiation for the redox reaction.

3.4. Preparation of SiO_2−TiO_2 Particulate Coatings. As discussed above, at a lower pH value (1−2) than the PZC of titania, the ST75 surface would become positively charged. The PZC is 2.1 for SiO_2,[25] and thus, at a pH value of 10, the SiO_2 surface would be negatively charged. Thus, uncalcinated ST75 nanoparticles (before calcination) or PDDA (cationic polyelectrolyte) can be deposited on the SiO_2 nanoparticle layer. In the following discussion, $(ST/S)_n$ is used to denote n deposition cycles of uncalcinated ST75 nanoparticles and a 20 nm SiO_2 nanoparticle bilayer. S_m is used to denote m deposition cycles of PDDA and a 20 nm SiO_2 nanoparticle bilayer. ST means one deposition layer of uncalcinated ST75 nanoparticles. Figure 5a−c shows SEM images of $(ST/S)_2$, $S_3(ST/S)_2$, and $S_3(ST/S)_2ST$ coatings, respectively. Clearly,

dx.doi.org/10.1021/am401124j | ACS Appl. Mater. Interfaces 2013, 5, 5282−5290

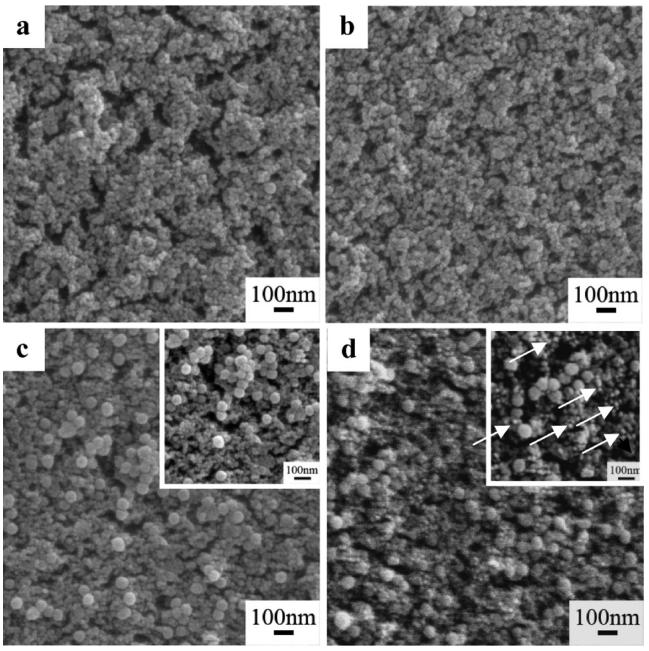

Figure 5. SEM images of $(ST/S)_2$ (a), $S_3(ST/S)_2$ (b), $S_3(ST/S)_2ST$ (c), and calcinated $S_3(ST/S)_2ST$ (550 °C for 3 h) (d), the insets are the corresponding magnified images of (c) and (d), respectively.

SiO_2 (20 nm) and ST75 core−shell (75 nm) nanoparticles before calcination were successfully assembled on slide glass. The $(ST/S)_2$ and $S_3(ST/S)_2$ coatings have the same surface layer of $(ST/S)_2$, and their SEM images show similar morphologies (Figure 5a,b). Comparing Figure 5b,c, ST75 nanoparticles without calcination were deposited uniformly on the $S_3(ST/S)_2$ surface. Atom force microscopy (AFM) observation was also carried out, and the result is shown in Figure S11 in the Supporting Information. ST75 nanoparticles existed on the $S_3(ST/S)_2ST$ surface without calcination, agreeing well with the SEM observation. The RMS roughness of $S_3(ST/S)_2ST$ without calcination was measured to be 14.7 nm. Figure 5d shows the morphology of $S_3(ST/S)_2ST$ coating calcinated at 550 °C for 3 h. Compared with the uncalcinated $S_3(ST/S)_2ST$ coating (Figure 5c), there were new ca.10 nm nanoparticles (pointed by white arrows) appearing on the $S_3(ST/S)_2ST$ coating after calcination. As discussed above from the TEM, DSC, and XRD results, these nanoparticles resulted from the transformation of amorphous TiO_2 shell.

3.5. Optical Properties of SiO_2−TiO_2 Particulate Coatings. The transmission spectra of slide glass, $(ST/S)_2$, $S_3(ST/S)_2$, and $S_3(ST/S)_2ST$ without calcination are shown in Figure 6a. The maximum transmittances of slide glass, $(ST/S)_2$, $S_3(ST/S)_2$, and $S_3(ST/S)_2ST$ were 91.3% (514 nm), 95.4% (539 nm), 96.2% (576 nm), and 95.7% (632 nm), respectively. Clearly, the maximum transmittance increases from $(ST/S)_2$ to $S_3(ST/S)_2$ with addition of three underlayers of 20 nm silica nanoparticles, and the transmittance decreases by further deposition of one layer of ST75 nanoparticles, indicating larger, more sparse ST75 nanoparticles are disadvantageous to antireflection at least partially due to the effect of light scattering. Figure 6b shows the transmission spectra of slide glass, $(ST/S)_2$, $S_3(ST/S)_2$, and $S_3(ST/S)_2ST$ after calcination at 550 °C for 3 h. It is noted that the transmittances were all enhanced as compared with those before calcination. The maximum transmittances of $(ST/S)_2$, $S_3(ST/S)_2$, and $S_3(ST/S)_2ST$ after calcination became 96.3% (528 nm), 97.1% (521 nm), and 97.3% (572 nm), respectively. This may be attributed to the transformation of amorphous titania shell to discrete anatase nanoparticles, which would result in the increase of film porosity. The maximum transmittance increased and all blue-shifted slightly, indicating the decrease of coating thickness, especially for $S_3(ST/S)_2ST$ from 95.7% at 632 nm to 97.3% at 572 nm.

Figure 7 shows the reflection spectra of slide glasses with the $(ST/S)_2$, $S_3(ST/S)_2$, and $S_3(ST/S)_2ST$ coatings after calcination at 550 °C for 3 h, respectively. All the coatings had lower reflectance than slide glass. The minimum reflectance of $S_3(ST/S)_2$ and $S_3(ST/S)_2ST$ coatings were ca. 0.89% (526 nm) and ca. 0.95% (601 nm), respectively, and are lower than that of the $(ST/S)_2$ coating (2.78% at 525 nm). Compared with the $S_3(ST/S)_2$ coating, the minimum reflectance of $S_3(ST/S)_2ST$

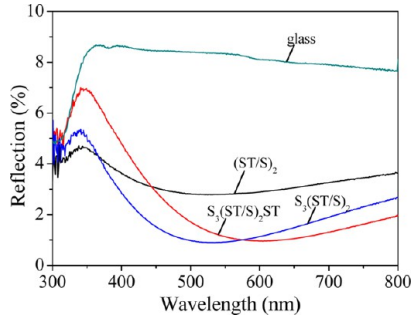

Figure 7. Reflection spectra of slide glasses with $(ST/S)_2$, $S_3(ST/S)_2$, and $S_3(ST/S)_2ST$ coatings, respectively, after calcination at 550 °C for 3 h.

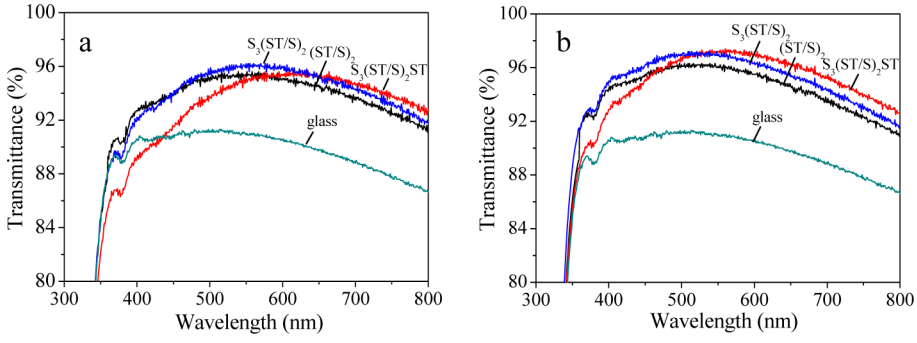

Figure 6. (a) Transmission spectra of slide glass, $(ST/S)_2$, $S_3(ST/S)_2$, and $S_3(ST/S)_2ST$ before calcination. (b) Transmission spectra of slide glass, $(ST/S)_2$, $S_3(ST/S)_2$, and $S_3(ST/S)_2ST$ after calcination at 550 °C for 3 h.

dx.doi.org/10.1021/am401124j | ACS Appl. Mater. Interfaces 2013, 5, 5282−5290

coating red-shifts from 526 to 601 nm. If a coating with a thickness (d_c) of $\lambda/4n_c$ (λ is the incident light wavelength) is to reach zero reflection, the refractive index of the coating should satisfy the criterion:

$$n_c = (n_a \times n_s)^{0.5} \quad (4)$$

where n_c, n_a, and n_s are the refractive indices of the coating, air, and substrate, respectively. Here, the value of n_a can be approximated as 1. For most glass and plastics, the value of n_s is ca. 1.5, and thus, the value of n_c could be calculated to be ca. 1.23.[23] The refractive indices of SiO_2 and TiO_2 (anatase) are 1.5 and 2.52. According this theory, the value of n_c must be reduced as close as possible to 1.23.

3.6. Wettability and Antifogging Properties. According to early theoretical works by Wenzel[42] and Quéré et al.,[43,44] void fraction and surface roughness would significantly affect the wettability of a surface with water. Before calcination, the WCAs of $(ST/S)_2$, $S_3(ST/S)_2$, and $S_3(ST/S)_2ST$ were 16.6°,12.7° and 10.6°, respectively. With increase of deposition cycles, the coatings became more hydrophilic. After calcination, these coatings showed superhydrophilic and antifogging properties, as shown by Figure 8. Generally, the super-

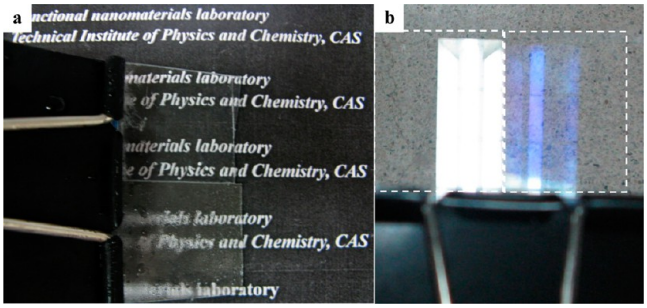

Figure 8. (a) Digital image exhibiting the antifogging property of slide glass deposited on both sides with calcinated $S_3(ST/S)_2ST$ (upper) together with control slide glass (lower). Both slides were cooled at ca. −15 °C for 3 h in a refrigerator and then exposed to boiling water vapor. (b) The reflection colors of slide glass (left) and that coated with $S_3(ST/S)_2ST$ and calcinated at 550 °C for 3 h (right).

hydrophilic properties of SiO_2 coatings are attributed to their high concentration of surface hydroxyl groups (Si−OH), high surface roughness, and voids which can absorb water, while the TiO_2 performance is augmented by its photochemical activity. The superhydrophilicity of SiO_2 coatings would, however, deteriorate when organics are adsorbed on the coating surface. The adsorption of organics would also lower the transmittance of coating. Coatings with only TiO_2 nanoparticles become superhydrophilic under UV radiation, but their transmittance is usually lower than that of SiO_2 coatings because of the high reflective index of TiO_2.[27] The wettability of raspberry-like SiO_2−TiO_2 nanoparticle coatings should result from the combined hydrophilic properties of SiO_2 and TiO_2, especially from SiO_2 in the absence of UV irradiation. Under UV irradiation, the photochemical activity of TiO_2 would enhance the hydrophilic property of the coatings.[27,45] The raspberry-like SiO_2−TiO_2 nanoparticle coatings also showed good antifogging property without UV radiation, especially $S_3(ST/S)_2ST$ (Figure 8a). This is because of the rough surface with high porosity and abundant Si−OH groups. Figure 8b shows the reflection colors of $S_3(ST/S)_2ST$ and slide glass, respectively. Clearly, the reflection of slide glass had been significantly suppressed by the $S_3(ST/S)_2ST$ coating.

3.7. Photocatalytic Property and Transmittance Recovery of Coatings. To explore the catalytic activity of SiO_2−TiO_2 raspberry-like nanoparticles, the degradation of MB in aqueous solution has been tested and discussed above. We also observed the degradation of MB adsorbed on theSiO_2−TiO_2 nanoparticle coating after calcination at 550 °C for 3 h. For the same coating sample, the photocatalytic test was repeated four times, and the coating showed good durable photocatalytic activity. As light transmission is a key issue of antireflective coatings, we depict the photocatalytic decomposition of MB adsorbed on the coating by transmission spectra. Figure 9a shows the transmittance spectra of slide glass with the SiO_2−TiO_2 nanoparticle coating under UV irradiation, which were recorded at the fourth photocatalytic test. Because of the adsorption of MB, the transmittance much decreased at 667 nm. During the UV irradiation, the MB adsorbed on the coating was gradually degraded, resulting in the increase in the transmittance of coated glass and its eventual recovery back to the value before the adsorption of MB. Figure 9b shows the transmittance recovery of $S_3(ST/S)_2ST$ coating (square) and slide glass (round). Different from the results observed under aqueous conditions (Figure S10, Supporting Information), MB adsorbed on blank slide glass could be degraded, and the transmittance of blank slide glass could recover over a longer period of time (40 min) to the transmittance before MB was adsorbed. The amounts of MB on the blank slide glass and the slide glass with $S_3(ST/S)_2ST$ coating are regarded as being the same because they had the same declination of transmittance

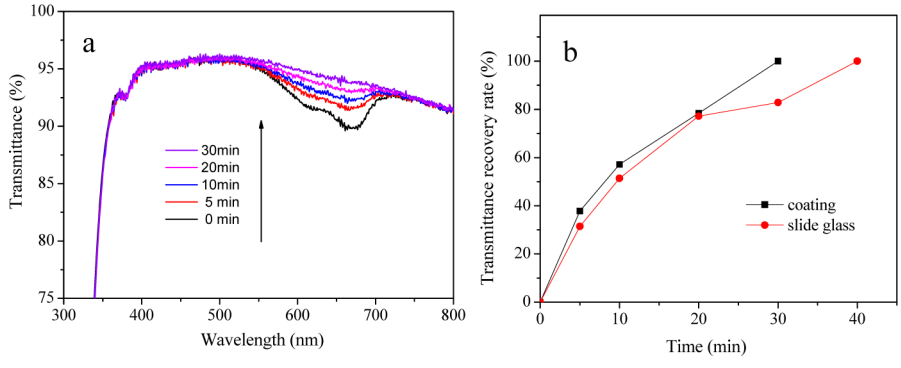

Figure 9. (a) Time-dependent transmission spectrum recovery of calcinated $S_3(ST/S)_2ST$ coating; (b) time-dependent percentage transmittance recovery at 667 nm of calcinated $S_3(ST/S)_2ST$ coating (square) and slide glass (round).

dx.doi.org/10.1021/am401124j | ACS Appl. Mater. Interfaces 2013, 5, 5282−5290

after the adsorption of MB. Due to the photocatalytic property of TiO_2 on the $S_3(ST/S)_2ST$ coating, only 30 min was needed for degrading the same amount of MB and recovering the transmittance. It is shorter than the degradation time of MB on the blank slide glass. Clearly, the slide glass with the coating had relatively faster kinetics than the blank slide glass, indicating better photocatalytic property and self-cleaning property of the coated slide glass. Such glasses with coatings could be applied as antireflective optical glasses with self-cleaning property, which can keep the self-cleaning property and high transmittance by degradation of organic materials adsorbed on the coating surface.[46]

Recently, Faustini et al. successfully fabricated SiO_2−TiO_2 two-layer nanoporous coatings by a facile sol−gel liquid deposition procedure,[47] which had excellent combined properties of antireflection, photocatalysis (self-cleaning), water repellence, and high water-wetting (antifogging). However, the maximum transmittance just had an increase of no more than 4%, which may be due to the limitation of coating structures. In contrast, the increase of more than 6% had been achieved in the maximum transmittance of coatings due to the flexibility of structural regulation of coating by the current LbL method.

4. CONCLUSIONS

In summary, a series of raspberry-like SiO_2−TiO_2 nanoparticles were prepared by a facile one-pot method and were used as a building block to fabricate self-cleaning and antireflective coatings. The size of TiO_2 nanoparticles on the surface of SiO_2 core could be controlled by tuning the TEOS/TIPT molar ratio. Coatings with both excellent photocatalytic self-cleaning and antireflective properties were prepared by alternate deposition of these SiO_2−TiO_2 nanoparticles and SiO_2 nanoparticles followed by calcination. The heat treatment transformed the amorphous TiO_2 shell into discrete anatase nanoparticles on the SiO_2 core, effectively avoided the TiO_2 nanoparticle agglomeration, and enhanced the transmittance.The maximum transmittance of calcinated coating reached as high as 97.3%. Under UV irradiation for 30 min, the transmittance of coated glass adsorbing MB could recover back to that of the coated glass without adsorbing MB, indicating excellent photocatalytic degradation of MB. The result means that the raspberry-like SiO_2−TiO_2 nanoparticle antireflective coatings have good photocatalytic decomposition toward organics and, thus, can keep their superhydrophilicity and high transmittances. These glasses with coatings may be applied on solar cell panels, green houses, and architectural glasses.

■ ASSOCIATED CONTENT

Supporting Information

TEM, FT-IR, XRD, and AFM characterization results. This material is available free of charge via the Internet at http://pubs.acs.org.

■ AUTHOR INFORMATION

Corresponding Author

*Tel/Fax: +86 10 82543535. E-mail: jhhe@mail.ipc.ac.cn.

Notes

The authors declare no competing financial interest.

■ ACKNOWLEDGMENTS

This work was supported by the National High Technology Research and Development Program ("863" Program) of China (Grant No. 2011AA050525), the Knowledge Innovation Program of the Chinese Academy of Sciences (CAS) (Grant Nos. KGCX2-YW-370, KGCX2-EW-304-2), and "Hundred Talents Program" of CAS.

■ REFERENCES

(1) O'Regan, B.; Grätzel, M. *Nature* **1991**, *353*, 737.
(2) Zukalová, M.; Zukal, A.; Kavan, L.; Nazeeruddin, M. K.; Liska, P.; Grätzel, M. *Nano Lett.* **2005**, *5*, 1789.
(3) Chiba, Y.; Islam, A.; Watanabe, Y.; Komiya, R.; Koide, N.; Han, L. *Jpn. J. Appl. Phys. 2* **2006**, *45*, 638.
(4) Bach, U.; Lupo, D.; Comte, P.; Moser, J.; Weissörtel, F.; Salbeck, J.; Spreitzer, H.; Grätzel, M. *Nature* **1998**, *395*, 583.
(5) Sauvage, F.; Di Fonzo, F.; Li Bassi, A.; Casari, C. S.; Russo, V.; Divitini, G.; Ducati, C.; Bottani, C. E.; Comte, P.; Graetzel, M. *Nano Lett.* **2010**, *10*, 2562.
(6) Chen, Q.; Xu, D. *J. Phys. Chem. C* **2009**, *113*, 6310.
(7) Inoue, T.; Fujishima, A.; Konishi, S.; Honda, K. *Nature* **1979**, *277*, 637.
(8) Park, J. H.; Kim, S.; Bard, A. J. *Nano Lett.* **2006**, *6*, 24.
(9) Khan, S. U. M.; Al-Shahry, M.; Ingler, W. B. *Science* **2002**, *297*, 2243.
(10) Yu, J.; Qi, L.; Jaroniec, M. *J. Phys. Chem. C* **2010**, *114*, 13118.
(11) Wolcott, A.; Smith, W. A.; Kuykendall, T. R.; Zhao, Y.; Zhang, J. Z. *Small* **2009**, *5*, 104.
(12) Ohko, Y.; Ando, I.; Niwa, C.; Tatsuma, T.; Yamamura, T.; Nakashima, T.; Kubota, Y.; Fujishima, A. *Environ. Sci. Technol.* **2001**, *35*, 2365.
(13) Wold, A. *Chem. Mater.* **1993**, *5*, 280.
(14) Riegel, G.; Bolton, J. R. *J. Phys. Chem.* **1995**, *99*, 4215.
(15) Hashimoto, K.; Irie, H.; Fujishima, A. *Jpn. J. Appl. Phys.* **2005**, *44*, 8269.
(16) Tayade, R. J.; Kulkarni, R. G.; Raksh, V. J. *Ind. Eng. Chem. Res.* **2006**, *45*, 922.
(17) Guo, C.; Ge, M.; Liu, L.; Gao, G.; Feng, Y.; Wang, Y. *Environ. Sci. Technol.* **2009**, *44*, 419.
(18) Wei, C.; Lin, W. Y.; Zainal, Z.; Williams, N. E.; Zhu, K.; Kruzic, A. P.; Smith, R. L.; Rajeshwar, K. *Environ. Sci. Technol.* **1994**, *28*, 934.
(19) Armelao, L.; Barreca, D.; Bottaro, G.; Gasparotto, A.; Maccato, C.; Maragno, C.; Tondello, E.; Štangar, U. L.; Bergant, M.; Mahne, D. *Nanotechnology* **2007**, *18*, 375709.
(20) Pinho, L.; Mosquera, M. J. *J. Phys. Chem. C* **2011**, *115*, 22851−22862.
(21) Pinho, L.; Mosquera, M. J. *Appl. Catal., B: Environ.* **2013**, *134*−*135*, 25−221.
(22) Roméas, V.; Pichat, P.; Guillard, C.; Chopin, T.; Lehaut, C. *New J. Chem.* **1999**, *23*, 365.
(23) Nakajima, A.; Koizumi, S.; Watanabe, T.; Hashimoto, K. *Langmuir* **2000**, *16*, 7048.
(24) Jimmy, C. Y.; Ho, W.; Lin, J.; Yip, H.; Wong, P. K. *Environ. Sci. Technol.* **2003**, *37*, 2296.
(25) Zhang, X. T.; Sato, O.; Taguchi, M.; Einaga, Y.; Murakami, T.; Fujishima, A. *Chem. Mater.* **2005**, *17*, 696.
(26) Wang, H.; Hu, Y.; Zhang, L.; Li, C. *Ind. Eng. Chem. Res.* **2010**, *49*, 3654.
(27) Zhang, X.; Fujishima, A.; Jin, M.; Emeline, A. V.; Murakami, T. *J. Phys. Chem. B* **2006**, *110*, 25142.
(28) Lee, D.; Rubner, M. F.; Cohen, R. E. *Nano Lett.* **2006**, *6*, 2305.
(29) Liu, X.; He, J. *J. Colloid Interface Sci.* **2007**, *314*, 341.
(30) Li, X.; Du, X.; He, J. *Langmuir* **2010**, *26*, 13528.
(31) Du, X.; Li, X. Y.; He, J. H. *ACS Appl. Mater. Interfaces* **2010**, *2*, 2365.
(32) Du, X.; He, J. H. *Chem.—Eur. J.* **2011**, *17*, 8165.
(33) Wang, C. C.; Ying, J. Y. *Chem. Mater.* **1999**, *11*, 3113.
(34) Zhang, Q.; Gao, L. *Langmuir* **2003**, *19*, 967.

(35) Ramakrishna, G.; Ghosh, H. N. *Langmuir* **2003**, *19*, 505.
(36) Stöber, W.; Fink, A.; Bohn, E. *J. Colloid Interface Sci.* **1968**, *26*, 62.
(37) Song, X.; Gao, L. *J. Phys. Chem. C* **2007**, *111*, 8180.
(38) Baolong, Z.; Baishun, C.; Keyu, S.; Shangjin, H.; Xiaodong, L.; Zongjie, D.; Kelian, Y. *Appl. Catal., B: Environ.* **2003**, *40*, 253.
(39) Li, W.; Ni, C.; Lin, H.; Huang, C. P.; Shah, S. I. *J. Appl. Phys.* **2004**, *96*, 6663.
(40) Lindgren, T.; Mwabora, J. M.; Avendaño, E.; Jonsson, J.; Hoel, A.; Granqvist, C. G.; Lindquist, S. E. *J. Phys. Chem. B* **2003**, *107*, 5709.
(41) Murugan, K.; Rao, T. N.; Gandhi, A. S.; Murty, B. S. *Catal. Commun.* **2010**, *11*, 518.
(42) Wenzel, R. *Ind. Eng. Chem.* **1936**, *28*, 988.
(43) Bico, J.; Marzolin, C.; Quéré, D. *Europhys. Lett.* **1999**, *47*, 220.
(44) Bico, J.; Tordeux, C.; Quéré, D. *Europhys. Lett.* **2001**, *55*, 214.
(45) Houmard, M.; Riassetto, D.; Roussel, F.; Bourgeois, A.; Berthomé, G.; Joud, J. C.; Langlet, M. *Appl. Surf. Sci.* **2007**, *254* (5), 1405.
(46) Carretero-Genevrier, A. n.; Boissiere, C. d.; Nicole, L.; Grosso, D. *J. Am. Chem. Soc.* **2012**, *134* (26), 10761.
(47) Faustini, M.; Nicole, L.; Boissière, C. d.; Innocenzi, P.; Sanchez, C.; Grosso, D. *Chem. Mater.* **2010**, *22* (15), 4406.